Published in final edited form as:
J Mol Recognit. 2013 April ; 26(4): 181–189. doi:10.1002/jmr.2263.

The Promiscuous Protein Binding Ability of Erythrosine B Studied by Metachromasy (Metachromasia)

Lakshmi Ganesan and **Peter Buchwald***
Department of Molecular and Cellular Pharmacology and Diabetes Research Institute, Miller School of Medicine, University of Miami, Miami, Florida, USA

Abstract

The present study aims to elucidate aspects of the protein binding ability of erythrosine B (ErB), a poly-iodinated xanthene dye and an FDA-approved food colorant (FD&C Red No. 3), which we have identified recently as a promiscuous inhibitor of protein–protein interactions (PPI) with a remarkably consistent median inhibitory concentration (IC_{50}) in the 5–30 μM range. Because ErB exhibits metachromasy, i.e., color change upon binding to several proteins, we exploited this property to quantify its binding to proteins such as bovine serum albumin (BSA) and CD40L (CD154) and to determine the corresponding binding constants (K_d) and stoichiometry (n_b) using spectrophotometric methods. Binding was reversible and the estimated affinities for both protein targets obtained here (K_d values of 14 and 20 μM for BSA and CD40L, respectively) were in good agreement with that expected from the protein–protein interaction (PPI) inhibitory activity of ErB. A stoichiometry greater than one was observed both for CD40L and BSA binding (n_b of 5–6 and 8–9 for BSA and CD40L, respectively) indicating the possibility of nonspecific binding of the flat an rigid ErB molecule at multiple sites, which could explain the promiscuous PPI inhibitory activity if some of these overlap with the binding site of the protein partner and interfere with the binding.

Keywords

bathochromic shift; erythrosine B; food colorants; metachromasia; promiscuous inhibitors; protein binding; protein-protein interactions

Introduction

During our ongoing search to identify small-molecule inhibitors of the CD40–CD40L (CD154) protein-protein interaction (PPI) (Margolles-Clark et al. 2009b; Margolles-Clark et al. 2009a; Buchwald et al. 2010; Margolles-Clark et al. 2010), a costimulatory interaction that plays an important role in adaptive immunity and hence is a therapeutic target of interest (Quezada et al. 2004; Elgueta et al. 2009), we have discovered that erythrosine B (ErB) is a relatively potent promiscuous PPI inhibitor (Ganesan et al. 2011). ErB is an FDA-approved food colorant (FD&C Red no. 3) with a poly-iodinated xanthene structure that seems to be a promiscuous, non-specific inhibitor of several PPI both within the tumor necrosis factor superfamily (TNFSF) as well as outside of it (e.g., EGFR–EGF) with a remarkably consistent activity, i.e., median inhibitory concentration, IC_{50}, in the 5–30 μM range.

*Corresponding Author: Peter Buchwald, Diabetes Research Institute, Miller School of Medicine, University of Miami, 1450 NW 10 Ave (R-134), Miami, FL 33136, USA, Tel.: 305 243-9657, pbuchwald@med.miami.edu.

Supporting Information. Purification of histidine tagged CD40L, verification if its trimeric status, and conformation of its activity in cell-free and cell-based assays. This material is available free of charge via the Internet.

Therefore, it was of obvious interest to attempt to elucidate the mechanistic aspects of the protein binding ability of ErB. Furthermore, small-molecule inhibition of PPIs is being increasingly pursued (Arkin and Wells 2004; Wells and McClendon 2007; Buchwald 2010; Mullard 2012), and being able to avoid promiscuous inhibitors is an important goal, just as it is in high-throughput strategies (HTS) that are often confounded by promiscuous inhibitors and frequent hitters (McGovern et al. 2002; Roche et al. 2002; Shoichet 2006). Fortunately, ErB is known to exhibit metachromasy, i.e., color change upon binding to several proteins, which has made it a useful diagnostic tool for the quantitative measurement of proteins in biological samples (Horikoshi et al. 2012) and we exploited this property to characterize its molecular binding to target proteins.

In general, metachromasy (or metachromasia), a term originating from Paul Ehrlich, is used to refer to a characteristic change in the color of staining in biological tissues, which is most typically exhibited by cationic dyes binding to particular substances (so-called chromotropes) present in these tissues (Michaelis and Granick 1945; Schubert and Hamerman 1956; Bergeron and Singer 1958; Stone 1967; Terada and Miyake 1973). For example, the basic (cationic) dye toluidine blue is a well-known example that becomes pink when bound to cartilage matrix. Some anionic (acidic) dyes, notably members of the eosin series, including erythrosine and fluorescein, are also known to exhibit weak metachromatic staining of polycations (e.g., histones, protamine); however, the corresponding color-shifts are typically much less than for cationic dyes and hence are not as useful for histological staining purposes (Prentø 2009). Metachromasy in organic dyes is typically observed upon concentration increase, temperature decrease, or in the presence of proteins or other large molecules. Whereas the first two are likely to result in dye aggregation altering its absorption pattern thereby causing a hue shift, the third involves binding to chromotropes (or chromoleptic substrates). In the latter case, the overall occupancy of the binding sites by dye molecules determines the extent of the observed color shift making it a convenient quantitative measure of molecular binding. Here, we report binding affinity (K_d, dissociation binding constant) and stoichiometry (n_b, number of binding sites per protein) data obtained by using spectrophotometric analysis of the metachromasy (color–shift) of ErB upon binding to representative proteins of interest such as bovine serum albumin (BSA) and CD40L (CD154).

Materials and Methods

Materials used for protein expression and purification as well as for the spectrophotometric analyses needed were as follows: pET-15b vector (Novagen, Madison, WI); restriction enzymes *BamHI* and *NdeI* (Promega, Madison, WI); Miller's LB agar (Difco; BD Biosciences, Franklin Lakes, NJ); terrific broth media (Affymetrix, Santa Clara, CA); isopropyl-β-D-1-thiogalactopyranoside (IPTG; Sigma–Aldrich, St. Louis, MO); EDTA-free protease inhibitor cocktail (Roche, Indianapolis, IN); nickel nitrilotriacetic acid (Ni-NTA) agarose resin (Qiagen, Valencia, CA); anti-CD40L monoclonal antibody (clone 4080)4; R&D Systems, MN), anti–$(His)_6$-tag antibody (Abcam, Cambridge, MA); gel filtration low molecular weight calibration kit (GE Healthcare Life Sciences, Piscataway, NJ). All other chemicals and reagents used were obtained from Sigma-Aldrich (St. Louis, MO).

Expression and Purification of Recombinant Human Histidine-Tagged Extracellular CD40L

Cloning of extracellular CD40L into pET-15b bacterial expression vector—

Nucleotides 357–812 from the cDNA of the full-length huCD40L (corresponding to amino acids 108–261 of extracellular domain) were PCR amplified using as forward primer 5' CTAGCATATGGAAAACAGCTTTGAAATGC 3' and as reverse primer 5' CTAGGGATCCTCAGAGTTTGAGTAAGCC 3'. This fragment was cloned into the multiple cloning site (MCS) of pET-15b vector (Novagen) under a T7 promoter and N-

terminal sequences for hexahistidine ($(His)_6$)–tag and thrombin cleavage. The restriction enzymes used were *BamHI* and *NdeI* (Promega).

Expression of histidine-tagged CD40L in E. coli—BL21 (pLys) S competent cells (Promega) were transformed with the cloned plasmid pET-15b described above and plated on Miller's LB agar (Difco; BD Biosciences). Colonies were selected for ampicillin resistance and introduced into Terrific Broth media (Affymetrix) for large-scale protein expression. The culture was grown in a bacterial shaker at 37°C and 250 rpm until the cells reached a density (OD_{600}) of 0.5 and switched to 30°C and 300 rpm before the addition of 1M isopropyl-β-D-1-thiogalactopyranoside (IPTG; Sigma–Aldrich), a lactose analog used to drive the expression of CD40L from the T7 promoter. After 4–6 h of expression, the bacterial cells were centrifuged, washed, and re-suspended in phosphate buffered saline (20 mM phosphate buffer, 500 mM NaCl) containing 20 mM imidazole and complete EDTA-free protease inhibitor cocktail (Roche) before their lysis by sonication.

Purification of histidine-tagged CD40L by Ni-NTA chromatography—The bacterial cell lysate was passed slowly through a column packed with nickel nitrilotriacetic acid (Ni-NTA) agarose resin (Qiagen). After collecting the flow-through, the column was washed with phosphate buffered saline (20 mM phosphate buffer, 500 mM NaCl) containing 20 mM imidazole until no protein emerged as observed using a Coomassie spot test. The column was progressively eluted with gradients of imidazole to eliminate non-specifically bound bacterial proteins having lower affinity. Pure $(His)_6$–tagged CD40L emerged upon addition of 250–300 mM imidazole, and the eluate was collected until no further protein emerged even after washing the column with 500 mM imidazole. The purity and identity was verified by SDS–PAGE (protein degradation products <10% of total) and by western blotting respectively (both using anti-CD40L monoclonal antibody (clone 4080)4; R&D Systems) and anti-$(His)_6$-tag antibody (Abcam). The concentration, C, of the pooled purified fractions was ascertained from absorbance, A, measured using NanoDrop 1000 spectrophotometer (Thermo-Fisher Scientific, Cambridge, MA) by setting the percent extinction coefficient (absorbance of 1% solution, $E_{1\%}$, w/v) of the protein at 280 nm to be 6.98, C (mg/mL) = 10 × ($A/E_{1\%}$) (Mazzei et al. 1995).

Purification of histidine-tagged CD40L by size exclusion chromatography—The fractions from nickel chromatography were further purified through a Superdex-200 size exclusion column (GE Healthcare Life Sciences) connected to ÄKTA™ fast protein liquid chromatography (FPLC) system (GE Healthcare Life Sciences). The protein was exchanged into 20 mM phosphate buffer, 500 mM NaCl, and 10% glycerol, used as the mobile phase at a flow rate of 0.5 mL/min to completely remove imidazole. Fractions were detected using an in-line UV detector set at wavelengths of 210, 280, and 260 nm to detect absorbance by peptide bonds, amino acids (Trp, Tyr, Cys), and nucleic acids, respectively. The apparent molecular weight of the purified $(His)_6$–tagged CD40L was ascertained from a calibration curve constructed using a gel filtration low molecular weight calibration kit (GE Healthcare Life Sciences).

CD40–CD40L binding assay—An ELISA-type assay, which was a modification of our previously described assay (Margolles-Clark et al. 2009b; Margolles-Clark et al. 2009a; Buchwald et al. 2010; Margolles-Clark et al. 2010; Ganesan et al. 2011), was used to confirm binding of the purified CD40L to its receptor, CD40. Briefly, microtiter plates (Nunc F Maxisorp; 96-well) were coated overnight at 4–8°C with 100 μL/well of Fc chimeric receptors diluted in PBS 7.2. This was followed by blocking with 200 μL/well of blocking solution (PBS 7.2, 0.05% Tween-20, 1% BSA) for 1 h at RT. The plates were then washed twice using the washing solution (PBS 7.4, 0.05% Tween-20) and dried before the

addition of various concentrations of ligand diluted in binding buffer (100mM HEPES, 0.005% BSA pH 7.2) to give a final volume of 100 μL/well. Anti-histidine tag antibody conjugated to horse radish peroxidase (HRP) or streptavidin-HRP conjugated antibodies was used to detect the bound CD40L. Plates were washed thrice before the addition of 120 μL/well of HRP substrate TMB (3,3',5,5'-tetramethylbenzidine) and kept in the dark for 30 min. The reaction was stopped using 30 μL 1M H_2SO_4, and the absorbance was read at 450 nm.

Activation of CD40L sensor cells—HEK-Blue™ CD40L sensor cells that can serve to measure the bioactivity of CD40L through the secretion of embryonic alkaline phosphatase (SEAP) upon NF-κB activation following CD40 stimulation were acquired from InvivoGen (San Diego, CA, USA). Cells were cultured and assayed for activation as recommended by the manufacturer. Briefly, the cells were cultivated in Dulbecco's Modified Eagle (DMEM) media supplemented with 4.5 g/L glucose, 10% v/v FBS, 50 U/mL penicillin, 50 μg/mL streptomycin, 100 μg/mL Normocin™, and 2 mM L-glutamine. The cells were centrifuged and re-suspended in the same medium without FBS, added to a 96-well microtiter plate at a density around 1×10^6 cells/well, and stimulated with various concentrations of CD40L diluted in the same media. After 24-h incubation at 37°C and 5% CO_2, SEAP levels were determined by adding QUANTI-Blue ™ reagent, whose change in color intensity from pink to purple/blue is proportional to the enzyme's activity. The level of SEAP was determined quantitatively using a spectrophotometer at 620–655 nm.

Metachromatic shift assay

Metachromasy assays were used to derive binding constants and stoichiometry for the dye–protein complex (D–P). The absorption spectra at various dye (ErB) concentrations (0 to 50 μM) with and without added protein (BSA, CD40L; 0 to 25 μM) were measured by spectrophotometry using SpectraMax M5 multi-label microplate reader (Molecular Devices LLC, Sunnyvale, CA) in the visible range (450 to 600 nm). Difference spectra were constructed by plotting the differences in optical density (OD) units of the spectral trace of free dye and that obtained for the same dye concentration in the presence of various concentrations of added protein. The difference in OD between the maximum and minimum points on the difference spectra was used as a quantitative measure of dye–protein complex formation for use in constructing binding curves and in analysis of stoichiometry (Bergeron and Singer 1958).

Binding curves

The amount of dye–protein complex (D–P) formed was quantified from the difference spectra as described above. Corresponding binding curves for different concentrations of added protein and dye were analyzed with GraphPad Prism version 6.01 (GraphPad, San Diego, CA) to obtain binding constants (K_d) and Hill coefficients (n_H) by fitting to a unified dose-response model corresponding to a general Hill equation (Klunk et al. 1999):

$$\frac{[D-P]}{[D-P]_{max}} = \frac{[D]^n}{[D]^n + {K_d}^n} = \frac{1}{1+10^{n_H(logK_d - log[D])}}$$

Two different analyses were used: in one, the raw, untransformed data from each series corresponding to a given protein P concentration were fitted with a model that used unified K_d and n_H values with variable maxima for each series, in the other one, data were normalized for each series using the corresponding maximum as 100% and data from all series were fitted with a single unified model.

Stoichiometry

Stoichiometry determinations were done using a Job's plot approach (Ingham 1975; MacCarthy 1978; Huang 1982; Schlein et al. 2001; Olson and Buhlmann 2011). In this approach, a measurable parameter that is proportional to the amount of complex formed is plotted as a function of the mole fraction composition and this is then used to determine the composition point where it is maximal. Here, the amount of dye-protein complex formed was quantified spectrophotometrically as described above (difference in OD between the maximum and minimum points on the difference spectra) and plotted at complementary molar ratios of dye and protein keeping the total molar concentration constant. Tangents were drawn from either side of the resultant plot to determine the point of maximum complex formation to give the stoichiometry (n_b, number of binding sites per protein) (Ingham 1975; MacCarthy 1978; Huang 1982; Schlein et al. 2001; Olson and Buhlmann 2011).

Results

To have sufficient protein for the binding experiments, CD40L was expressed with a hexa-histidine $(His)_6$–tagging in *Escherichia coli* and purified using nickel-NTA affinity chromatography as described in the Materials and Methods section. The purity of the CD40L was verified by SDS-PAGE (protein degradation products <10% of total), and the concentration was determined using a NanoDrop spectrophotometer. A concentration of 13.6 mg/mL of >95% pure CD40L protein was obtained (Suppl. Figure S1). To assess the molecular size and hence the oligomer status of the purified CD40L, the pure fractions collected from the nickel column were subjected to size exclusion chromatography, which separates proteins based on their hydrodynamic radius. The apparent molecular weight inferred with a calibration curve constructed using a gel filtration low molecular weight calibration kit indicated it to be a trimer (i.e., molecular weight of approximately 50 kDa) (Suppl. Figure S2), consistent with evidence in the literature showing CD40L to form stable, active trimers (Mazzei et al. 1995) just as other members of the TNF superfamily that are thought to be active primarily in trimeric form, either on the cell surface or soluble after extracellular cleavage (Aggarwal 2003; Croft et al. 2012). We verified that the purified histidine-tagged CD40L binds its receptor (CD40) in a dose-dependent manner using our ELISA-based binding assay developed earlier (Margolles-Clark et al. 2009a; Ganesan et al. 2011) (Suppl. Figure S3). Furthermore, the ability of the purified histidine-tagged CD40L to activate CD40-mediated NF-κB transactivation was confirmed using HEK-Blue CD40L sensor cell as described in the Materials and Methods section (Suppl. Figure S3). The absence of activation of a CD40-null line was used as a control to demonstrate the specificity of activation.

To study the protein binding ability of ErB, which seems to be a promiscuous and non-specific protein-protein interaction inhibitor (Ganesan et al. 2011), we selected bovine serum albumin (BSA) and CD40L as representative targets mainly because ErB exhibited a clear spectral shift (metachromasy) upon binding to them (Prentø 2009). Increasing concentrations of added BSA and CD40L produced a progressive bathochromic shift (red-shift, i.e., shift to longer wavelengths) in the spectra of ErB (Figure 1, Figure 2). The wavelength of maximum absorption (λ_{max}) shifted from 527 nm in the absence of protein to 536 nm and 531 nm in the presence of 25 μM BSA and CD40L, respectively. The bathochromic shift (red-shift) caused by BSA as observed here was in agreement with previous observations (Mathavan et al. 2009; Zhang and Görner 2009), and it was larger than the one caused by CD40L. A hypochromic shift (shift to a lower intensity) was also observed upon addition of both proteins with the shift caused by BSA being somewhat less pronounced than that caused by CD40L (Figure 1 vs. Figure 2). These metachromatic shifts

were used to quantify the complex formation between ErB and its protein binding partners, BSA and CD40L, respectively as described in the Materials and Methods section.

The binding constants (K_d) obtained for ErB here by fitting these data with standard Hill-equation based binding models were 14 μM and 20 μM for BSA and CD40L, respectively (Figure 3). These values are in excellent agreement with our previous observation that ErB acts as a promiscuous PPI inhibitor with a remarkably consistent IC_{50} in the 5–30 μM range. Notably, in both cases here the binding curves had Hill slopes (n_H) significantly different from unity, 2.05(±0.09) and 2.41(±0.10) for ErB–BSA and ErB–CD40L binding, respectively, indicative of the presence of some cooperativity.

Using the presence of metachromatic shift, we also investigated the stoichiometry of these bindings, i.e., whether there is multiple binding sites for ErB on these proteins, by applying a Job's plot analysis (Ingham 1975; Huang 1982; Schlein et al. 2001; Olson and Buhlmann 2011). This analysis is based on the principle that for mixtures of varying compositions, maximum complex formation occurs at the right stoichiometry. The Job plots were constructed using complementary molar ratios of dye and protein (BSA and CD40L) such that the total molar content remained constant. The amount of dye-protein complex formed for a given condition was quantified from spectral data as described previously, and the points of maximum complex formation were derived from the tangents drawn from both ends (Figure 4, Figure 5). Maximum complex formation (i.e., best stoichiometry) was found to occur at 85:15 ratio for the ErB–BSA complex (n_b of 5–6 ErB molecules per BSA, Figure 4) and at 90:10 for the ErB–CD40L complex (8–9 ErB molecules per CD40L, Figure 5).

Discussion

While searching for small-molecule PPI inhibitors for receptor-ligand pairs in the TNF superfamily (Margolles-Clark et al. 2009b; Margolles-Clark et al. 2009a; Buchwald et al. 2010; Margolles-Clark et al. 2010), we observed that erythrosine B (ErB), an FDA-approved food colorant (FD&C Red No. 3), acts as a relatively potent ($IC_{50} \approx 2–20$ μM) and non-specific PPI inhibitor (Ganesan et al. 2011). This was in agreement with its long-known inhibitory activity, within the same concentration range, on various other protein interactions or activities, such as dopamine uptake, acetylcholine release, drug transporters and metabolizing enzymes (CYP34A, UGT1A6 (Mizutani 2009), insulin–insulin receptor interaction, and many others (see (Ganesan et al. 2011) and references therein). Among the six FDA approved food colorants (Glória 2006), this inhibitory activity seems to be unique for ErB, but rose Bengal (RB), a structural analog and food colorant approved in Japan, showed similar, maybe even more pronounced, promiscuous inhibitory activity (Ganesan et al. 2011). In agreement with this non-specific inhibitory activity ErB showed cytotoxic effects around this concentration range ($IC_{50} \approx 50$ μM) in the cell lines tested (THP-1, Jurkat, and HEK-293T), an effect that was even more pronounced with its chlorinated analog RB (Ganesan et al. 2011). ErB was also recently also shown to cause genotoxicity at concentrations ≥ 50 μM using a hepatocellular carcinoma HepG2 cell line (Chequer et al. 2012). Hence, an obvious concern related to this promiscuous inhibitory activity is the possibility of toxic side effects in humans, especially as a number of possible behavioral alterations and food allergies have been often – and controversially – linked to food colorants (MacGibbon 1983), and this is likely to become an increasingly important issue since, for example, in the US, the use of food dyes increased about five-fold since 1955 and currently about 100 tons of ErB are produced annually and certified by the FDA (Kobylewski and Jacobson 2010). The current acceptable daily intake (ADI) for ErB is 0.1 mg/kg body weight/day (Gardner et al. 1987; JECFA 1991; EFSA 2011), already considerably lower than that of any other FDA-approved food color [e.g., 7 mg/kg body weight/day for allura red or 7.5 for tartrazine (Glória 2006)]. As we have discussed before

(Ganesan et al. 2011), because the nonspecific inhibitory activity of ErB starts to become a concern at concentrations in the 2–20 μM (approx. 2–20 mg/L) range, related effects should not be an issue if the ADI guidelines (0.1 mg/kg body weight/day) are followed. It is further reassuring that according to recent estimates, the current levels of use intake estimates of ErB for adults in the European Union (EU) on average is only 0.0031 mg/kg body weight/day (with 0.01 mg/kg body weight/day at the 95th percentile); hence, they are well below the ADI of 0.1 (EFSA 2011). However, it has to be noted that in the EU, ErB is approved only for limited applications (use in cocktail and candied cherries, and Bigarreaux cherries) contrary to the US, where it is approved as a coloring in general foods.

Since ErB is a member of the eosin series and is among the relatively few anionic dyes that exhibit color change (metachromasy) upon complex formation (McKay and Hillson 1965; Prentø 2009), we explored this property to study the affinity and stoichiometry of its protein binding using spectrophotometric methods with BSA and CD40L as representative targets. Increasing concentrations of added protein did indeed produce a progressive bathochromic (red) shift in the absorption spectra of ErB (Figure 1, Figure 2) and quantification of the corresponding data suggested binding affinities of 15–20 μM for both proteins, in excellent agreement with our previous observation that ErB acts as a promiscuous PPI inhibitor with a remarkably consistent IC_{50} in exactly this range (Ganesan et al. 2011). The value obtained here for ErB–BSA binding (14 μM) is also in good agreement with values published previously, which were also in the low micromolar range (Jang et al. 1985; Kim et al. 1987; Mathavan et al. 2009). The binding curves obtained here for both proteins (Figure 3) had Hill slope, n_H, values significantly different from unity hinting at the presence of double cooperativity ($n_H \approx 2$) in the nature of the interaction causing the metachromatic red-shift. Binding as a dimer could be a possibility, some evidence for this for ErB–BSA has been found previously in fluorescence quenching experiments (Zhang and Görner 2009).

Availability of a spectrophotometric approach also allowed us to study the stoichiometry of the protein binding of ErB (i.e., the number of ligands bound per protein), and we used a Job plot type approach. This is a continuous variation method, in which a measurable parameter that is proportional to the amount of complex formed is plotted as a function of the ligand: receptor mole fraction composition while keeping the total ligand + receptor molar concentration constant and then used to determine the composition point where it is maximal (Ingham 1975; MacCarthy 1978; Huang 1982; Schlein et al. 2001; Olson and Buhlmann 2011). Here, the amount of dye–protein complex formed was quantified from the difference between the maximum and minimum extremes of the ΔOD difference spectra (Figure 1, Figure 2) as described above and then plotted at complementary molar ratios of dye (ErB) and protein (Figure 4 for BSA and Figure 5 for CD40L). In both cases, multiple ErB molecules seem to bind to the protein target: our estimates indicate 5 to 6 ErB molecules per BSA molecule and possibly 8 to 9 ErB molecules per CD40L. The more skewed the stoichiometry the less accurate the estimate has to be considered, but the value obtained here for ErB–BSA binding is in good agreement with a previous value of $n_b = 6$ obtained by Jang, Kim, and co-workers using a spectrophotometric approach but a different quantitation method (Jang et al. 1985; Kim et al. 1987). Zhang and Görner found a biphasic Scatchard plot for ErB–BSA binding suggesting the possibility of two distinct binding modes, one with n_{b1} of 4 and another with n_{b2} of 8 (and corresponding to K_ds of 1 and 10 μM, respectively) (Zhang and Görner 2009).

These observations for both CD40L and BSA binding indicate the possibility of binding of ErB molecule at multiple sites with low micromolar affinity, which could account for the promiscuous PPI inhibitory activity observed in the very same concentration range (Ganesan et al. 2011) assuming that some of the ErB bound overlaps with the binding site of the protein partner and interfere with the binding. A similar mechanism has already been

suggested for the inhibition of the insulin–insulin receptor PPI by ErB via reversible binding at multiple binding sites on the protein surface at least one of which overlaps with the binding site of the protein partner (Schlein et al. 2001; Schlein et al. 2002).

From this perspective, it is important that ErB, as well as some of its analog such as rose Bengal that also showed promiscuous PPI inhibitory activity, are relatively large, flat, and rigid structures that have no rotatable bonds, especially in their spiro isomeric forms, so that they can easily bind to flat, hydrophobic pockets on the protein surface (Ganesan et al. 2011). Entropy and more specifically loss of entropy due to binding plays a critical role in modulating binding efficiency, but predicting its contribution is non-trivial and controversial (Murray and Verdonk 2002; Tirado-Rives and Jorgensen 2006; Reynolds et al. 2008). The barrier to binding due to the loss of rigid–body entropy varies across a considerable range (Reynolds et al. 2007), its value being somewhere around 15–20 kJ/mol, which corresponds to about three orders of magnitude in affinity, according to a more recent estimate (Murray and Verdonk 2002). This might explain at least partially, the promiscuous binding activity of ErB: a relatively large, flat molecule with a rigid structure capable of van der Waals interactions (including aromatic stacking) with no entropy loss due to blocking of rotational freedoms. Presence of large halogen (iodine) substituents also seems important for the non-specific inhibitory activity: within xanthene analogs of ErB explored, there was a clear trend indicating that the smaller the size the less prominent the promiscuous inhibitory activity (Ganesan et al. 2011). Since these xanthene dyes (ErB, RB) are well-known photosensitizers that might bind non-covalently and enhance photosensitized oxidation of biomolecules (Mignaco et al. 1997; Davies 2003; Zhang and Görner 2009), photosensitization might account for some of the inhibiting activity. Our inhibitory assays carried out in dark vs. light conditions in parallel found the activity of ErB and RB to diminish in dark about 5 to 10-fold, but most of the activity is still retained in dark.

In summary, metachromasy studied allowed us to better characterize quantitatively the binding of ErB to protein targets such as BSA and CD40L. These studies indicate that ErB is likely to bind with low micromolar affinity at multiple sites on the surface of these proteins. This can interfere with the binding of the protein partner and is likely to be the main mechanism behind the nonspecific, promiscuous PPI inhibitory activity of ErB, which is observed in the same concentration range of 5–30 μM (approximately 5–30 mg/L).

Supplementary Material

Refer to Web version on PubMed Central for supplementary material.

Acknowledgments

We would like to thank Dr. Vladlen Z. Slepak, Dr. Konstantin Levay, and Darla Karpinsky (University of Miami, Molecular and Cellular Pharmacology Department) as well as Dr. Nancy Vargas (University of Miami, Diabetes Research Institute) for their help in the preparation and purification of CD40L.

Funding Sources

This work was supported by the National Institutes of Health National Institute of Allergy and Infectious Diseases Grant 1R01AI101041-01 (P. Buchwald)

Abbreviations

BSA	bovine serum albumin
ErB	erythrosine B

HTS	high throughput screening
IC_{50}	median inhibitory concentration
K_d	equilibrium dissociation constant
PPI	protein–protein interaction
RB	rose Bengal
TNFSF	tumor necrosis factor superfamily

References

Aggarwal BB. Signalling pathways of the TNF superfamily: a double-edged sword. Nat. Rev. Immunol. 2003; 3:745–756. [PubMed: 12949498]

Arkin MR, Wells JA. Small-molecule inhibitors of protein-protein interactions: progressing towards the dream. Nat. Rev. Drug Discov. 2004; 3:301–317. [PubMed: 15060526]

Bergeron JA, Singer M. Metachromasy: an experimental and theoretical reevaluation. J. Biophys. Biochem. Cytol. 1958; 4:433–457. [PubMed: 13563551]

Buchwald P. Small-molecule protein-protein interaction inhibitors: therapeutic potential in light of molecular size, chemical space, and ligand binding efficiency considerations. IUBMB Life. 2010; 62:724–731. [PubMed: 20979208]

Buchwald P, Margolles-Clark E, Kenyon NS, Ricordi C. Organic dyes as small molecule protein–protein interaction inhibitors for the CD4–CD154 costimulatory interaction. J. Mol. Recognit. 2010; 23:65–73. [PubMed: 19621420]

Chequer FMD, Venâncio VP, Bianchi MLP, Antunes LMG. Genotoxic and mutagenic effects of erythrosine B, a xanthene food dye, on HepG2 cells. Food Chem. Toxicol. 2012; 50:3447–3451. [PubMed: 22847138]

Croft M, Duan W, Choi H, Eun SY, Madireddi S, Mehta A. TNF superfamily in inflammatory disease: translating basic insights. Trends Immunol. 2012; 33:144–152. [PubMed: 22169337]

Davies MJ. Singlet oxygen-mediated damage to proteins and its consequences. Biochem. Biophys. Res. Commun. 2003; 305:761–770. [PubMed: 12763058]

EFSA Panel on Food Additives and Nutrient Sources Added to Food (ANS). Scientific opinion on the re-evaluation of Erythrosine (E 127) as a food additive. EFSA J. 2011; 9:1854.

Elgueta R, Benson MJ, de Vries VC, Wasiuk A, Guo Y, Noelle RJ. Molecular mechanism and function of CD40/CD40L engagement in the immune system. Immunol. Rev. 2009; 229:152–172. [PubMed: 19426221]

Ganesan L, Margolles-Clark E, Song Y, Buchwald P. The food colorant erythrosine is a promiscuous protein-protein interaction inhibitor. Biochem. Pharmacol. 2011; 81:810–818. [PubMed: 21219880]

Gardner DF, Utiger RD, Schwartz SL, Witorsch P, Meyers B, Braverman LE, Witorsch RJ. Effects of oral erythrosine (2',4',5',7'-tetraiodofluorescein) on thyroid function in normal men. Toxicol. Appl. Pharmacol. 1987; 91:299–304. [PubMed: 2447681]

Glória, MBA. Synthetic Colorants. In: Hui, YH., editor. Handbook of food science, technology, and engineering. Boca Raton: CRC Press; 2006. 86-1-86-15

Horikoshi S, Higurashi A, Kaneko E, Yoshimura H, Ohsawa I, Suzuki Y, Hamada C, Tomino Y. A new screening method for proteinuria using Erythrosin B and an automated analyzer - rapid, sensitive and inexpensive determination. Clin. Chim. Acta. 2012; 413:1087–1091. [PubMed: 22465201]

Huang CY. Determination of binding stoichiometry by the continuous variation method: the Job plot. Methods Enzymol. 1982; 87:509–525. [PubMed: 7176926]

Ingham KC. On the application of Job's method of continuous variation to the stoichiometry of protein-ligand complexes. Anal. Biochem. 1975; 68:660–663. [PubMed: 1200365]

Jang SK, Kim B-K, Lee W-K. Studies on the interaction of edible dyes with protein I: Binding parameters of edible dyes with bovine serum albumin. Arch. Pharm. Res. 1985; 8:169–175.

JECFA (Joint FAO/WHO Expert Committee on Food Additives). Evaluation of Certain Food Additives and Contaminants, 37th Report. Geneva: World Health Organization; 1991.

Kim B-K, Lah WL, Jang SK, Lim BH, Jang JY, Lee W-K. Studies on the interaction of edible dyes with protein II: The effects of drug additions on protein binding of edible dyes. Arch. Pharm. Res. 1987; 10:29–35.

Klunk WE, Jacob RF, Mason RP. Quantifying amyloid by Congo red spectral shift assay. Methods Enzymol. 1999; 309:285–305. [PubMed: 10507031]

Kobylewski, S.; Jacobson, ME. Food Dyes A Rainbow of Risks. Washington, DC: Center for Science in the Public Interest; 2010. p. 58

MacCarthy P. Simplified experimental route for obtaining Job's curves. Anal. Chem. 1978; 50:2165.

MacGibbon B. Adverse reactions to food additives. Proc. Nutr. Soc. 1983; 42:233–240. [PubMed: 6351081]

Margolles-Clark E, Kenyon NS, Ricordi C, Buchwald P. Effective and specific inhibition of the CD40-CD154 costimulatory interaction by a naphthalenesulphonic acid derivative. Chem. Biol. Drug Des. 2010; 76:305–313. [PubMed: 20636329]

Margolles-Clark E, Umland O, Kenyon NS, Ricordi C, Buchwald P. Small molecule costimulatory blockade: organic dye inhibitors of the CD40-CD154 interaction. J. Mol. Med. 2009a; 87:1133–1143. [PubMed: 19707732]

Margolles-Clark E, Jacques-Silva MC, Ganesan L, Umland O, Kenyon NS, Ricordi C, Berggren P-O, Buchwald P. Suramin inhibits the CD40–CD154 costimulatory interaction: a possible mechanism for immunosuppressive effects. Biochem. Pharmacol. 2009b; 77:1236–1245. [PubMed: 19283894]

Mathavan VMK, Boh BK, Tayyab S. Characterization of erythrosine B binding to bovine serum albumin and bilirubin displacement. Indian J. Biochem. Biophys. 2009; 46:325–331. [PubMed: 19788065]

Mazzei GJ, Edgerton MD, Losberger C, Lecoanet-Henchoz S, Graber P, Durandy A, Gauchat JF, Bernard A, Allet B, Bonnefoy JY. Recombinant soluble trimeric CD40 ligand is biologically active. J. Biol. Chem. 1995; 270:7025–7028. [PubMed: 7706236]

McGovern SL, Caselli E, Grigorieff N, Shoichet BK. A common mechanism underlying promiscuous inhibitors from virtual and high-throughput screening. J. Med. Chem. 2002; 45:1712–1722. [PubMed: 11931626]

McKay RB, Hillson PJ. Metachromatic behaviour of dyes in solution - Interpretation on basis of interaction between dye ions and counter-ions. Trans. Faraday Soc. 1965; 61:1800–1810.

Michaelis L, Granick S. Metachromasy of basic dyestuffs. J. Am. Chem. Soc. 1945; 67:1212–1219.

Mignaco JA, Barrabin H, Scofano HM. ATPase and phosphatase activities are differentially inhibited by photo-oxidation of the sarcoplasmic reticulum Ca(2+)-ATPase. Biochim. Biophys. Acta. 1997; 1321:252–258. [PubMed: 9393643]

Mizutani T. Toxicity of xanthene food dyes by inhibition of human drug-metabolizing enzymes in a noncompetitive manner. J. Env. Publ. Health. 2009; 2009:953952.

Mullard A. Protein-protein interaction inhibitors get into the groove. Nat. Rev. Drug Discov. 2012; 11:173–175. [PubMed: 22378255]

Murray CW, Verdonk ML. The consequences of translational and rotational entropy lost by small molecules on binding to proteins. J. Comput. Aided Mol. Des. 2002; 16:741–753. [PubMed: 12650591]

Olson EJ, Buhlmann P. Getting more out of a Job plot: determination of reactant to product stoichiometry in cases of displacement reactions and n:n complex formation. J. Org. Chem. 2011; 76:8406–8412. [PubMed: 21895009]

Prentø P. Staining of macromolecules: possible mechanisms and examples. Biotech. Histochem. 2009; 84:139–158. [PubMed: 19384746]

Quezada SA, Jarvinen LZ, Lind EF, Noelle RJ. CD40/CD154 interactions at the interface of tolerance and immunity. Annu. Rev. Immunol. 2004; 22:307–328. [PubMed: 15032580]

Reynolds CH, Bembenek SD, Tounge BA. The role of molecular size in ligand efficiency. Bioorg. Med. Chem. Lett. 2007; 17:4258–4261. [PubMed: 17532632]

Reynolds CH, Tounge BA, Bembenek SD. Ligand binding efficiency: trends, physical basis, and implications. J. Med. Chem. 2008; 51:2432–2438. [PubMed: 18380424]

Roche O, Schneider P, Zuegge J, Guba W, Kansy M, Alanine A, Bleicher K, Danel F, Gutknecht EM, Rogers-Evans M, Neidhart W, Stalder H, Dillon M, Sjogren E, Fotouhi N, Gillespie P, Goodnow R, Harris W, Jones P, Taniguchi M, Tsujii S, von der Saal W, Zimmermann G, Schneider G. Development of a virtual screening method for identification of"frequent hitters" in compound libraries. J. Med. Chem. 2002; 45:137–142. [PubMed: 11754585]

Schlein M, Ludvigsen S, Olsen HB, Dunn MF, Kaarsholm NC. Spectroscopic characterization of insulin and small molecule ligand binding to the insulin receptor. Spectroscopy. 2002; 16:147–159.

Schlein M, Ludvigsen S, Olsen HB, Andersen AS, Danielsen GM, Kaarsholm NC. Properties of small molecules affecting insulin receptor function. Biochemistry. 2001; 40:13520–13528. [PubMed: 11695899]

Schubert M, Hamerman D. Metachromasia; chemical theory and histochemical use. J. Histochem. Cytochem. 1956; 4:159–189. [PubMed: 13306945]

Shoichet BK. Screening in a spirit haunted world. Drug Discov. Today. 2006; 11:607–615. [PubMed: 16793529]

Stone AL. Aggregation of cationic dyes on acid polysaccharides. II. Quantitative parameters on metachromasy. Biochim. Biophys. Acta. 1967; 148:193–206. [PubMed: 6077037]

Terada H, Miyake K. Interaction of organic dyes and proteins - determination of the binding constants spectrophotometrically. Kolloid Z. u. Z. Polymere. 1973; 251:139–145.

Tirado-Rives J, Jorgensen WL. Contribution of conformer focusing to the uncertainty in predicting free energies for protein-ligand binding. J. Med. Chem. 2006; 49:5880–5884. [PubMed: 17004703]

Wells JA, McClendon CL. Reaching for high-hanging fruit in drug discovery at protein-protein interfaces. Nature. 2007; 450:1001–1009. [PubMed: 18075579]

Zhang Y, Görner H. Photoprocesses of xanthene dyes bound to lysozyme or serum albumin. Photochem. Photobiol. 2009; 85:677–685. [PubMed: 19076304]

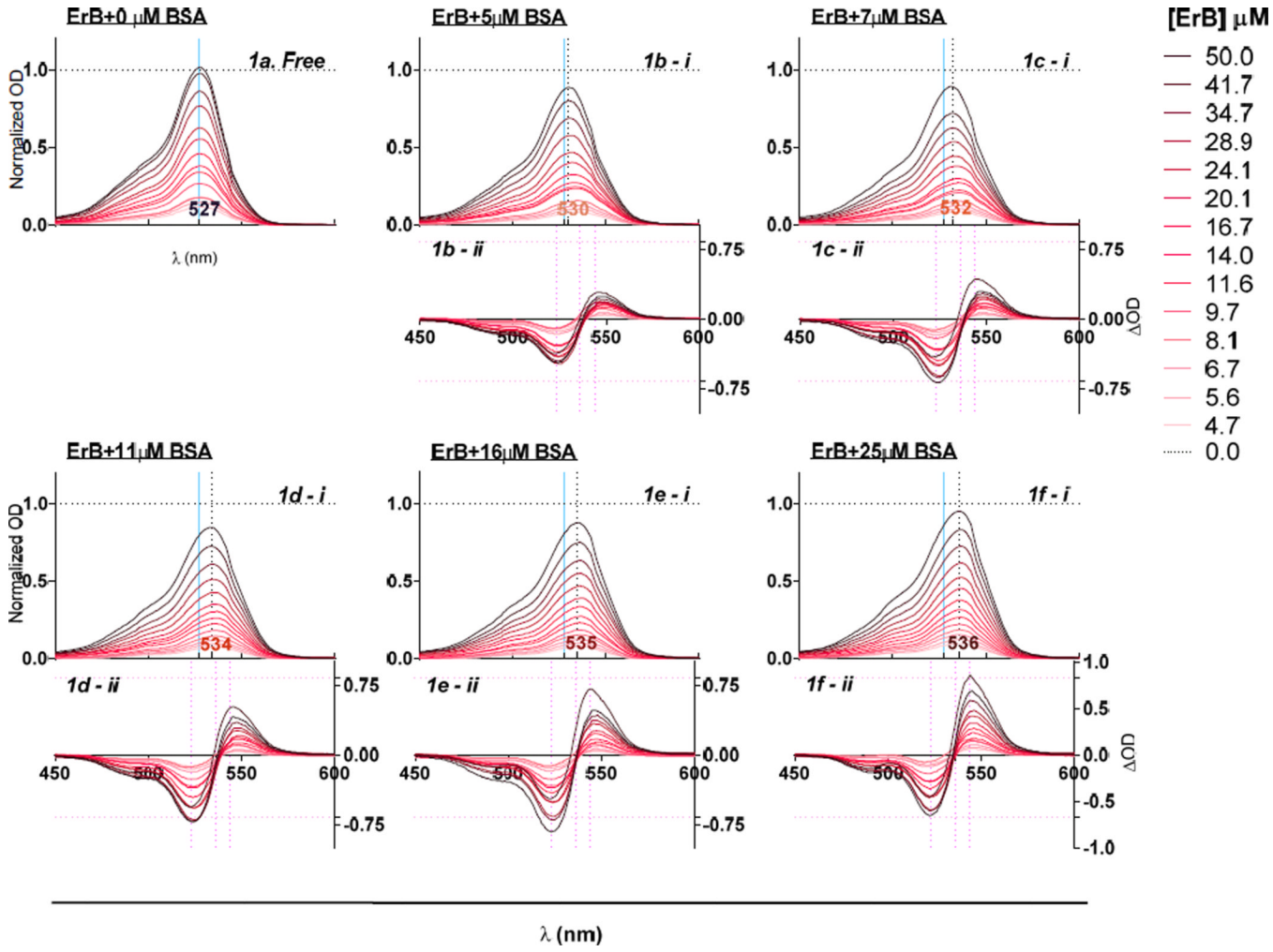

Figure 1.

Metachromatic shift in erythrosine B spectra in the presence of various concentrations of BSA. Absorbance spectra of different concentrations of ErB with 0 μM BSA [a]; 5 μM BSA [b - i]; 7 μM BSA [c - i]; 11 μM BSA [d - i]; 16 μM BSA [e - i]; and 25 μM BSA [f - i] showing spectral shift from a λ_{max} of 527 nm obtained without added protein (0 μM BSA). Data shown are normalized OD calculated as OD normalized to OD_{max} obtained with free dye. Difference spectra of ErB (calculated as the difference compared to that in the absence of protein, i.e. 0 μM BSA) with 5 μM BSA [b - ii]; 7 μM BSA [c - ii]; 11 μM BSA [d - ii]; 16 μM BSA [e - ii]; and 25 μM BSA [f - ii].

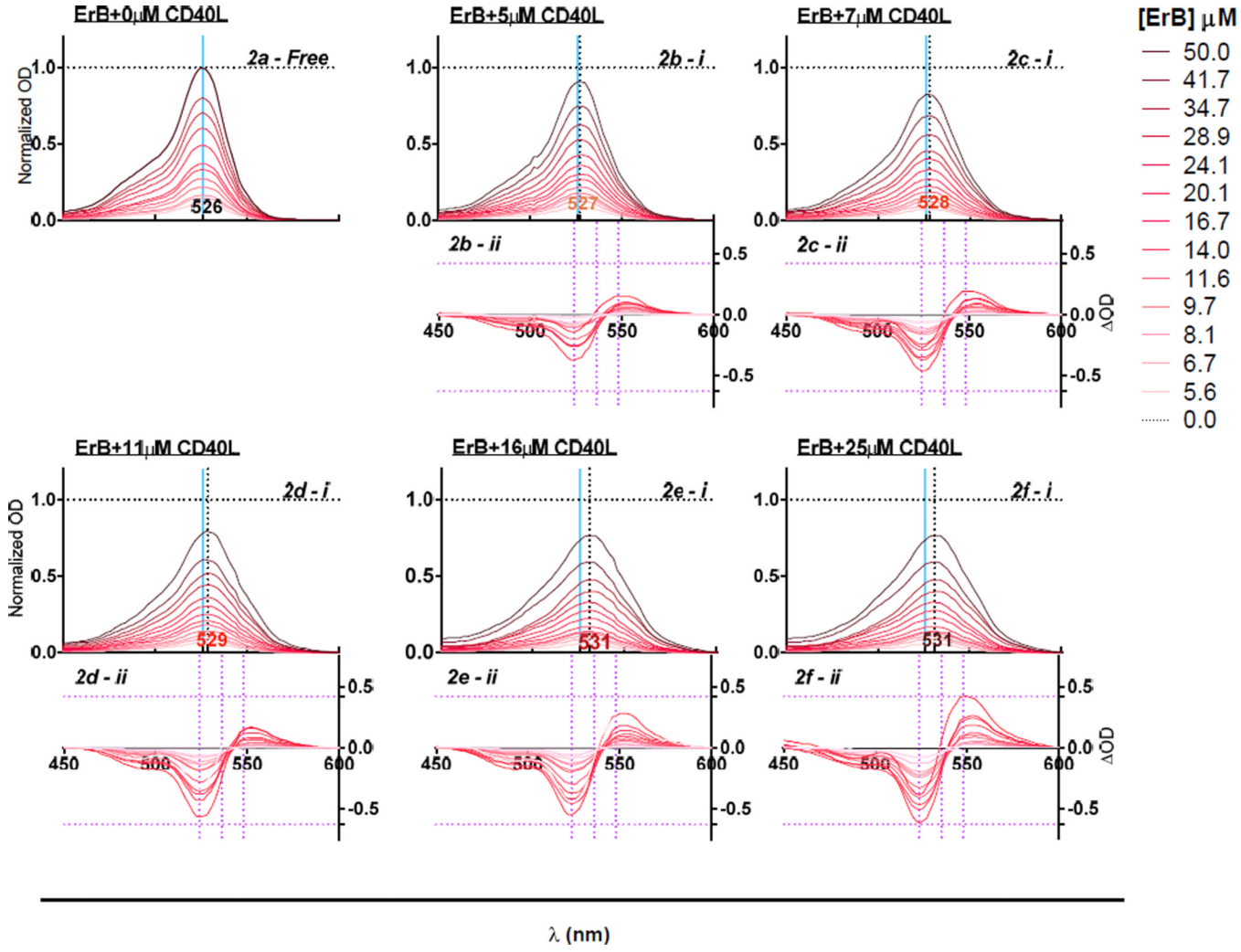

Figure 2.

Metachromatic shift in erythrosine B spectra in the presence of various concentrations of CD40L. Absorbance spectra of different concentrations of ErB with 0 μM CD40L [a]; 5 μM CD40L [b - i]; 7 μM CD40L [c - i]; 11 μM CD40L [d - i]; 16 μM CD40L [e - i]; and 25 μM CD40L [f - i] showing spectral shift from a λ_{max} of 527 nm obtained without added protein (0 μM BSA). Data shown are normalized OD calculated as OD normalized to OD_{max} obtained with free dye. Difference spectra of ErB (calculated as the difference compared to that in the absence of protein, i.e. 0 μM CD40L) with 5 μM CD40L [b - ii]; 7 μM CD40L [c - ii]; 11 μM CD40L [d - ii]; 16 μM CD40L [e - ii]; and 25 μM CD40L [f - ii].

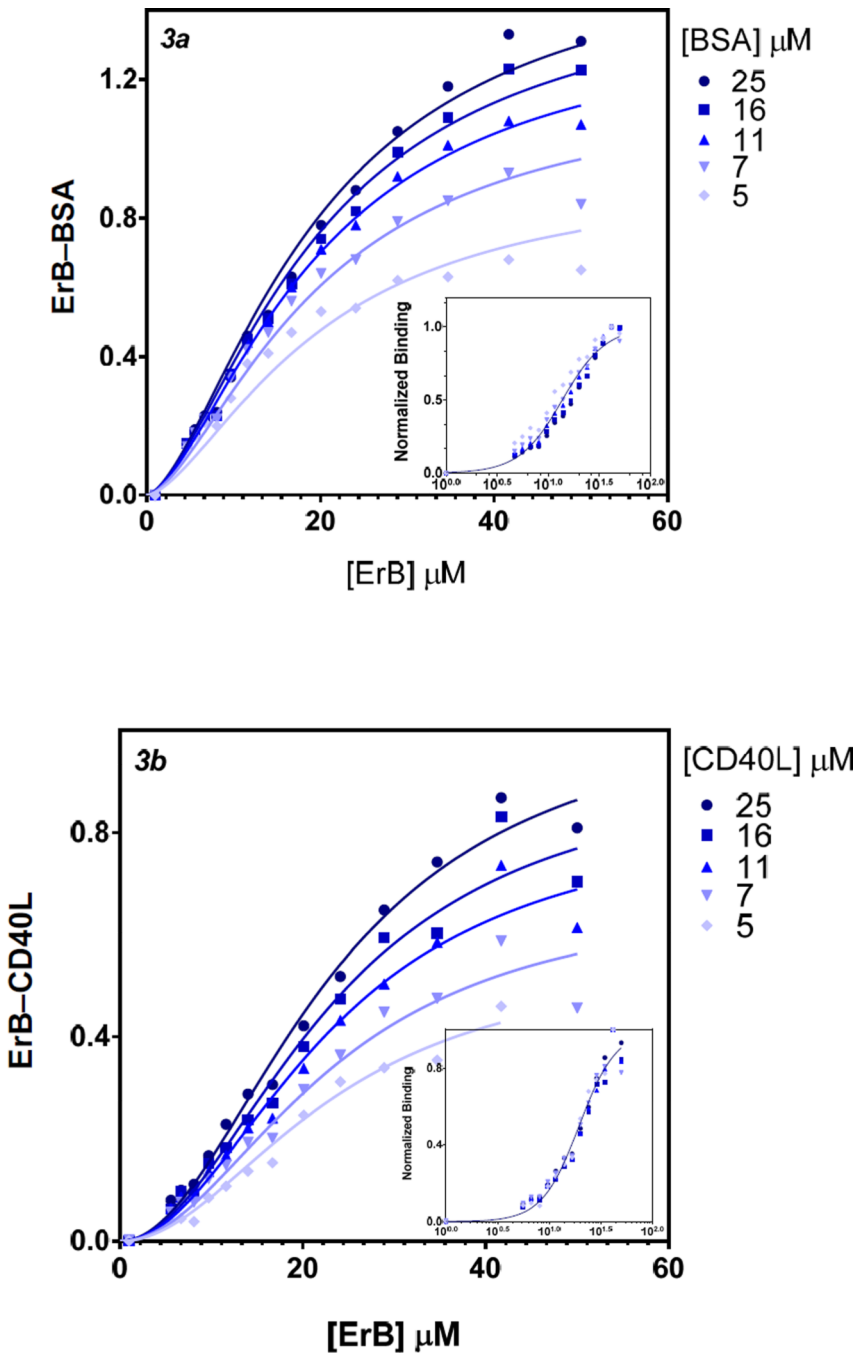

Figure 3.

Binding curves obtained from the metachromatic shift data for ErB to BSA (a) and CD40L (b), respectively. Symbols show the experimental data obtained in the presence of various concentrations of BSA or CD40L with the lines indicating the fit obtained with a Hill equation type general dose-response model (GraphPad Prism) using unified binding constant (K_d) and Hill slope (n_H) values across series. Insets show the same data normalized for each series and fit with a single model using a semi-log scale.

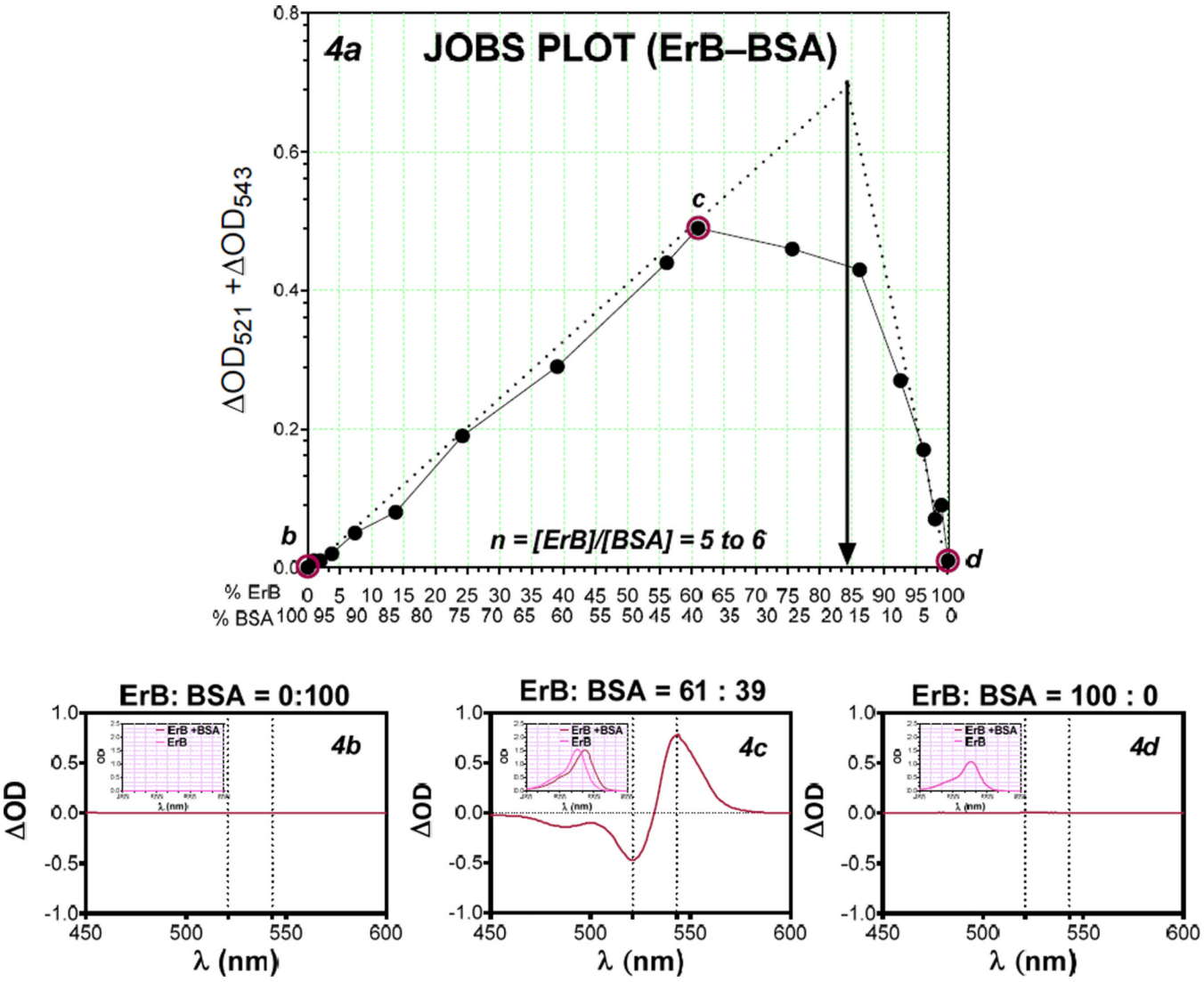

Figure 4.

Job's plot of ErB–BSA binding. Plot of BSA-caused metachromatic shift data obtained at complementary molar ratios of ErB and BSA keeping the total molar content constant to allow estimation of the stoichiometry (*n*) of complex formation [a]. The corresponding difference spectra of BSA protein with no added ErB (50 μM BSA + 0 μM ErB) [b], BSA with some added ErB (19.5 μM BSA + 30.5 μM ErB) [c], and ErB with no added BSA (0 μM BSA + 50 μM ErB) [d] with insets showing the corresponding absorbance spectra are included for illustration.

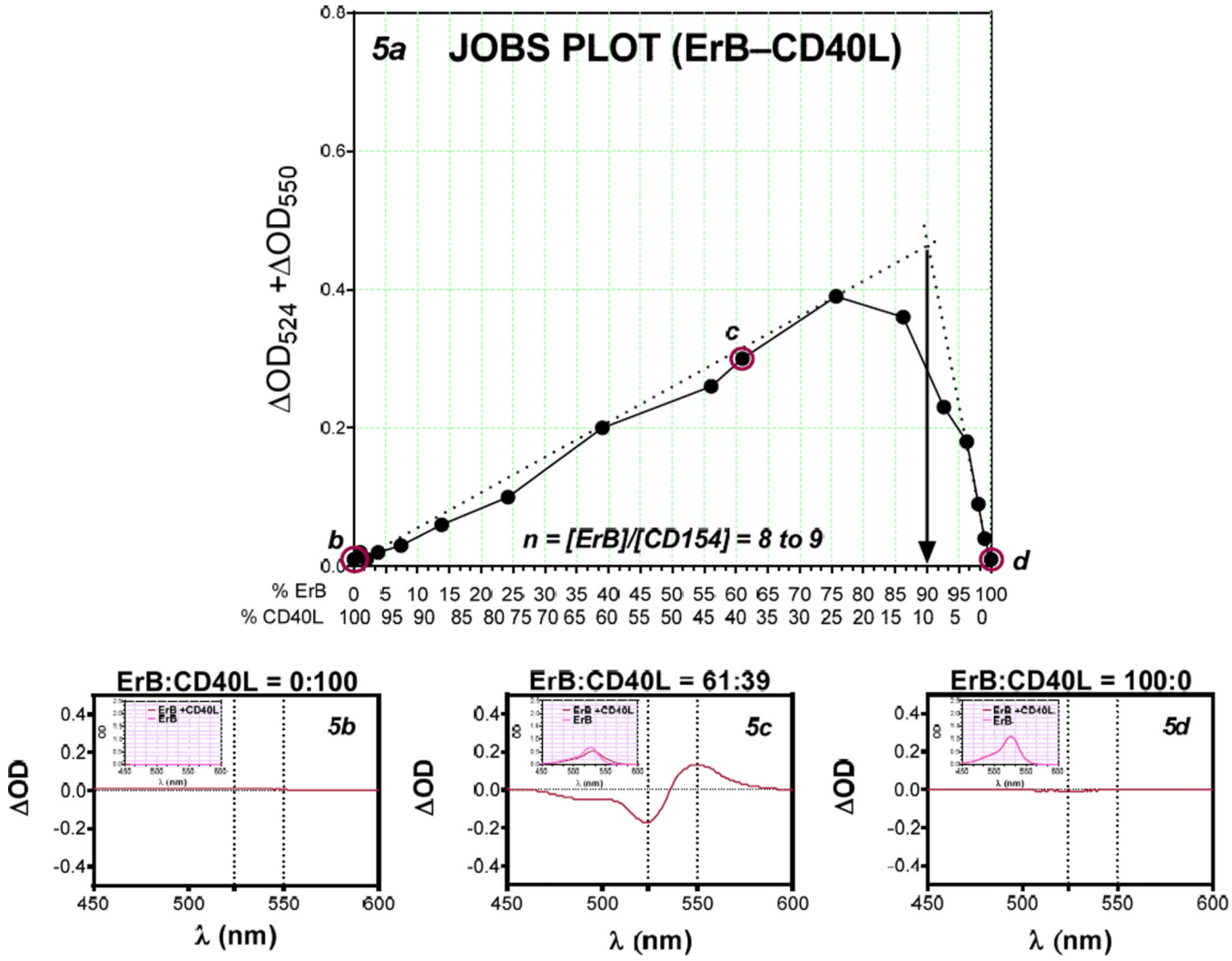

Figure 5.

Job's plot of ErB–CD40L binding. Plot of CD40L-caused metachromatic shift data obtained at complementary molar ratios of ErB and CD40L keeping the total molar content constant to allow estimation of the stoichiometry (*n*) of complex formation [a]. The corresponding difference spectra of CD40L protein with no added ErB (50 μM CD40L+ 0 μM ErB) [b], CD40L with some added ErB (19.5 μM CD40L + 30.5 μM ErB) [c], and ErB with no added CD40L (0 μM CD40L + 50 μM ErB) [d] with insets showing the corresponding absorbance spectra are included for illustration.